# A 300 mK ultra-high vacuum scanning tunneling microscope for spin-resolved spectroscopy at high energy resolution

J. Wiebe,[a] A. Wachowiak,[b] F. Meier, and D. Haude
*Institute of Applied Physics and Microstructure Research Center, University of Hamburg, Jungiusstr. 11, 20355 Hamburg, Germany*[c]

T. Foster
*Oxford Instruments Superconductivity, Tubney Woods, Oxon OX13 5QX, United Kingdom*

M. Morgenstern[d] and R. Wiesendanger
*Institute of Applied Physics and Microstructure Research Center, University of Hamburg, Jungiusstr. 11, 20355 Hamburg, Germany*[c]

(Received 19 May 2004; accepted 25 July 2004; published 1 November 2004)

We describe the design and development of a scanning tunneling micoscope (STM) working at very low temperatures in ultra-high vacuum (UHV) and at high magnetic fields. The STM is mounted to the $^3$He pot of an entirely UHV compatible $^3$He refrigerator inside a tube which can be baked out to achieve UHV conditions even at room temperature. A base temperature of 315 mK with a hold time of 30 h without any recondensing or refilling of cryogenics is achieved. The STM can be moved from the cryostat into a lower UHV-chamber system where STM-tips and -samples can be exchanged without breaking UHV. The chambers contain standard surface science tools for preparation and characterization of tips and samples in particular for spin-resolved scanning tunneling spectroscopy (STS). Test measurements using either superconducting tips or samples show that the system is adequate for performing STS with both high spatial and high energy resolution. The vertical stability of the tunnel junction is shown to be 5 $pm_{pp}$ and the energy resolution is about 100 $\mu$eV. © *2004 American Institute of Physics.* [DOI: 10.1063/1.1794431]

## I. INTRODUCTION

The unique power of scanning tunneling spectroscopy (STS) is its ability to give direct access to the local density of states (LDOS) of the electron system of solid surfaces, which is measured energetically resolved and with subnanometer spatial resolution.[1] While the high spatial resolution is caused by the principle of operation of the scanning tunneling microscope (STM) itself, a high energy resolution is only possible at low temperatures.[2,3] However, STS-measurements with high energy resolution are necessary to study effects where the interaction of the electron system plays a major role, because these effects are mostly determined by small energy scales. Since interaction effects often cause a spatial reorganization of the electron system, STS as a local method allows insight into the physics of interacting electron systems.

Some interaction effects like charge density waves,[4,5] the Kondo effect,[6–8] high-$T_C$ superconductivity,[9,10] or magnetism[11–14] have already been investigated by STS at temperatures between 4 K and room temperature. Many other interaction effects of great interest, however, demand temperatures below 1 K and have not yet been extensively studied. Examples are the fractional quantum Hall effect,[15] metal-insulator transitions in two-dimensional electron systems,[16] superconductivity in heavy fermion compounds,[17,18] or *p*-wave superconductivity in systems like $Sr_2RuO_4$.[19–21]

Even for effects that appear at higher temperatures, STS profits from the higher energy resolution achieved in the subkelvin regime. Thus, very small energy scales would be easily resolvable. An example is the Rashba splitting in two-dimensional electron systems which is typically of the order of a few millielectron volts in InAs inversion layers.[22–24] Finally, the high energy resolution permits mapping of single wave functions in extended systems that are dense in energy on larger length scales.[25–29] For example, single drift states of the quantum Hall phase could be mapped with a localization length that is a factor of 5 larger than at 6 K.[26] This allows for experimental investigation of wave function properties which were only theoretically accessible up to now.[30] Subkelvin temperatures thus open up a whole range of new fields of research that can be explored by STS.

While STMs working at temperatures around 4 K became standard in the last couple of years, there are only few reports of STMs with a base temperature in the subkelvin range. These facilities use either $^3$He evaporation cryostats[31–35] or dilution refrigerators.[21,36–40] The main problem is the difficulty to combine STM as an extremely vibration sensitive method with the mechanical pumps usually necessary for the cooling process. Furthermore, a high magnetic field is often desired as an easily accessible parameter which

[a]Author to whom correspondence should be addressed; electronic mail: jwiebe@physnet.uni-hamburg.de
[b]Present address: Department of Physics, University of California at Berkeley, Berkeley, CA 94720-7300.
[c]Electronic mail: http://www.nanoscience.de/group_r/
[d]Present address: II. Inst. of Physics B, RWTH Aachen University, Physikzentrum Melaten, Huyskensweg, 52056 Aachen, Germany.

 

can be used to tune the interaction effects of the electron system relative to the kinetic energy. High field magnets constrict the sample space diameter to a few centimeters, requiring a very compact design of the STM. Finally, for quantitative STS or spin-resolved STS, an atomically clean sample surface and tip apex is necessary. Thus sample and tip have to be prepared in ultrahigh vacuum (UHV). Pan *et al.*[33] obtained very convincing STS results on high-$T_C$ superconductors[9,41,42] by utilizing the cryogenic vacuum of the cryostat to achieve UHV condition. However, this method is restricted to sample systems which can be prepared by cleavage in the cryogenic vacuum. Many surfaces and hybrid structures require more elaborate preparation steps like molecular beam epitaxy which have to be carried out in UHV. For these structures, the sample has to be transferred from the preparation chamber to the STM without breaking the UHV state. The only facilities so far which combine the above demands are the $^3$He refrigerated STMs by Kugler *et al.*[34,43] and Heinrich *et al.*[35] and the dilution refrigerated STM by Matsui *et al.*[39,40]

We have succeeded in building a $^3$He refrigerated STM which permits STS measurements with high spatial and energy resolution in the presence of high magnetic fields. Samples and tips can be exchanged and transferred under true UHV conditions throughout an extensive UHV system equipped with standard surface science methods for sample and tip preparation and characterization. In particular, the *in situ* tip exchange is essential for the preparation of thin film tips to be used for spin-resolved STS measurements.[11,44,45] The performance of the facility is demonstrated by test measurements using ferromagnetic and superconducting samples as well as ferromagnetic and superconducting tips.

## II. INSTRUMENT DESIGN

In order to achieve an energy resolution in STS measurements close to the thermal limit both the mechanical and the electrical noise levels have to be reduced as far as possible. To limit the mechanical noise level, we concentrated on three major points. First, we built an external vibration isolation which decouples the cryostat from the surroundings to reduce noise from outside the experiment. Second, we used a $^3$He evaporation cryostat with a noiseless $^3$He sorption pump. Third, the STM head itself is compact and rigid and fairly insusceptible to vibrations. Additional internal vibration isolation is thus not necessary. These major points will be described below.

Figure 1 shows an overview of the facility. The main part is a $^3$He evaporation refrigerator in a bottom loading cryostat (1) with a superconducting magnet which contains the low temperature STM. The STM can be lowered from the measuring position inside the cryostat into the central chamber (7) for sample- and tip exchange without leaving UHV. From there, they can be transferred into the two neighboring UHV chambers (8,9) for preparation and characterization.

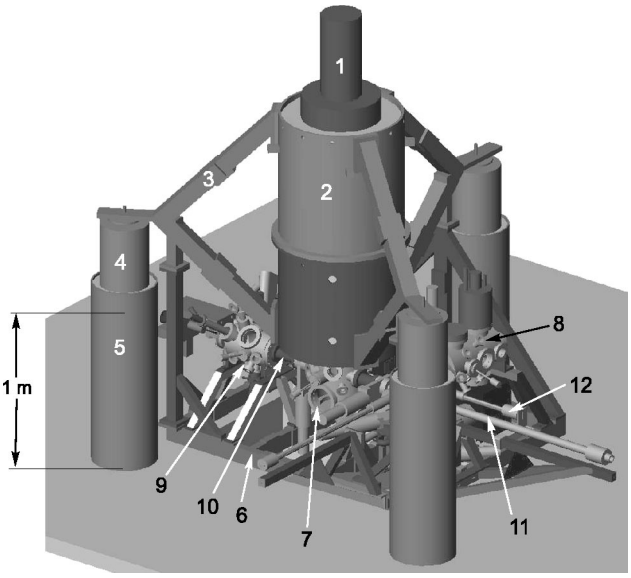


FIG. 1. Overview of the facility. (1) Bottom loading cryostat containing the $^3$He refrigerator, the low temperature STM and the superconducting magnet, (2) sand-filled aluminum barrel, (3) stainless-steel supports filled with sand, (4) air springs, (5) sand-filled supporting legs, (6) sand-filled stainless-steel frame mounted to the supports (3), (7) central UHV chamber for sample and tip exchange from the low temperature STM, (8) second UHV chamber containing a room temperature STM, molecular beam evaporators, and a combined LEED/Auger-system, (9) third UHV chamber containing a variable-temperature MOKE-setup, the tip and sample heater, molecular beam evaporators, and an ion source, (10) edge-welded bellows, (11) magnetic linear and rotary motion drives, and (12) load lock.

### A. External vibration isolation

The design of the facility was optimized to reach high mechanical stability of the whole setup. Although the system with its three UHV chambers is relatively extensive, we obtained a compact design by using three support points and an angular arrangement of the chambers. This and the large mass of 2.5 t makes the setup fairly insensitive to vibrations. The facility itself rests on the foundation in the basement of our building. The cryostat is decoupled from the floor using a three-stage damping system: First, the dewar is embedded in a sand-filled aluminum barrel (2) which screens the walls of the cryostat against sound from the surroundings. Since the cryostat is bottom loading, the sand bed has to be provided with an aperture for the base flange as can be seen in Fig. 2. A rubber ring (4) prevents the sand from leaking out. It is at the same time flexible enough to ensure that the base plate of the cryostat rests mainly on sand. Secondly, the three supports (3) (see Fig. 1) which carry the barrel rest on air springs (4) with a resonance frequency of about 1 Hz. These absorb the remaining vibrations with a frequency above several Hertz. Third, the air springs are supported on a sand layer having a depth of 1 m which is kept within the supporting legs (5). These legs support the frame far above its center of gravity for better stability of the air damping system.

Furthermore, the complete base frame consisting of the supports (3) and the frame (6) is constructed of hollow sections filled with sand to effectively damp sound. Finally, the central UHV chamber (7), which is mounted to the bottom flange of the cryostat, is mechanically decoupled from the

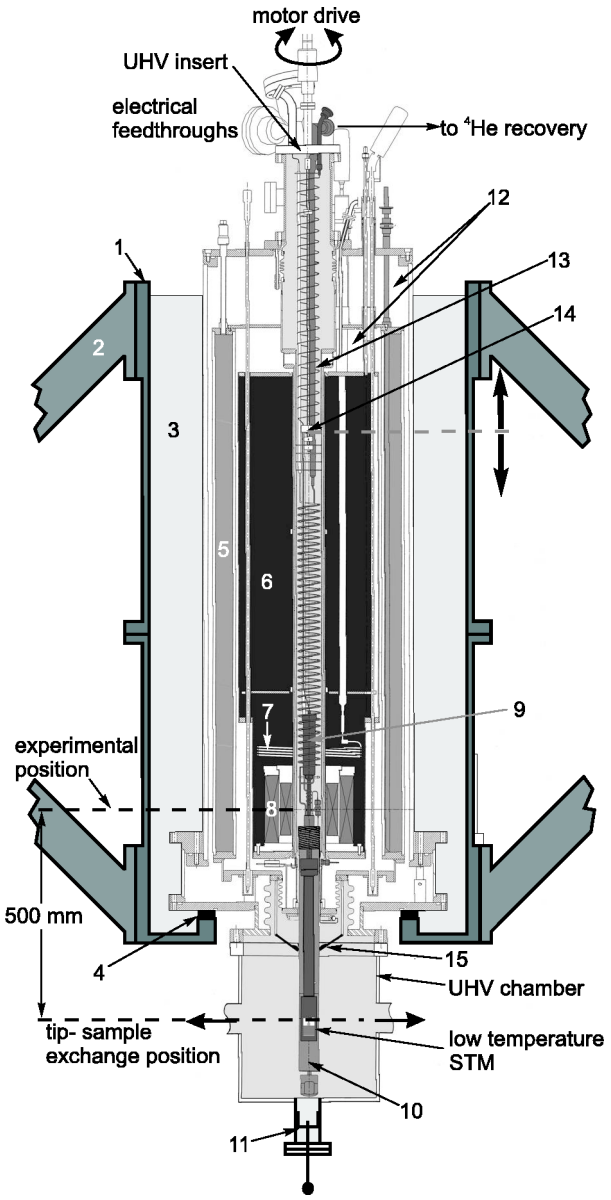


FIG. 2. The bottom loading cryostat with the $^3$He refrigerator. The UHV insert is shown in the fully extended position with the STM moved into the UHV chamber for tip or sample exchange. (1) Aluminum barrel, (2) stainless-steel supports, (3) sand, (4) rubber ring, (5) liquid nitrogen bath, (6) $^4$He dewar, (7) lambda fridge, (8) 12/14T magnet, (9) single-shot $^3$He refrigerator, (10) radiation shield, (11) UHV rotary feedthrough for opening the radiation shield (10), (12) isolation vacuum, (13) threaded leadscrew, (14) aluminum-bronze nut, and (15) radiation flaps at 77 K.

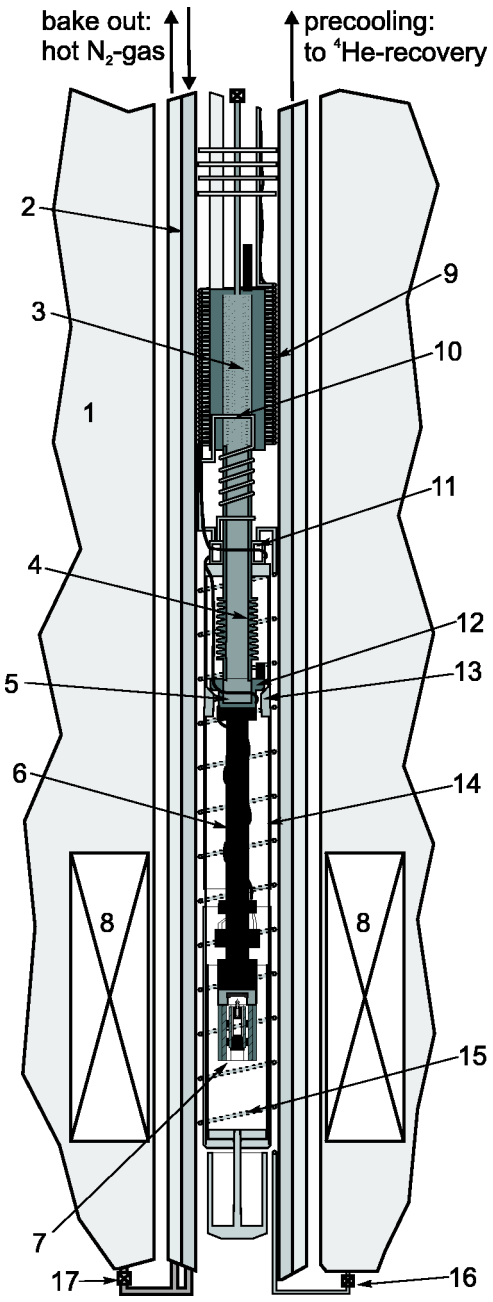


FIG. 3. $^3$He refrigerator in experimental position. (1) $^4$He bath, (2) baking/cooling tubes, (3) charcoal sorption pump, (4) flexible bellow, (5) $^3$He pot, (6) OFHC-copper rod, (7) STM, (8) superconducting magnet, (9) $^4$He exhaust capillary, (10) bypass for sorption pump cooling, (11) 1 K pot, (12) cone of $^3$He pot, (13) countercone thermally coupled to 1 K pot, (14) radiation shield, (15) 1 K-pot feeding-capillary, (16) 1 K-pot needle-valve, and (17) baking/cooling-tubes needle-valve.

two other UHV chambers (8,9), which are fixed to the frame, by the use of edge-welded bellows (10).

### B. Cryogenics, thermometry and magnet

The $^3$He evaporation refrigerator, which was designed and built by Oxford Instruments Superconductivity,[51] is an enhanced version of the cryostat used by Kugler *et al.*[34,43] It was designed with the aim of a long base temperature hold time adequate for time-consuming STS measurements, an easy and fast sample exchange during which the STM stays cold, and a refrigeration technique that minimizes vibrations. As opposed to the Kugler system, in our cryostat the entire $^3$He refrigerator including the STM can be baked out to achieve UHV conditions even with the cryostat at room temperature.

Figure 2 shows a section through the cryostat. It comprises a 77 $\ell$ liquid $^4$He- and a 56 $\ell$ liquid nitrogen dewar (6,5) which is superinsulated in a surrounding isolation vacuum (12). The superconducting solenoid (8) with a 77 mm bore provides a maximum field of 12 T perpendicular to the sample surface at 4.2 K. A lambda fridge (7) can be used to cool the magnet to 2.2 K in order to achieve a field of 14 T. The sample in the STM head is placed in the center

of the homogeneous region (0.3% over a 10 mm diameter spherical volume) of the field.

The $^3$He refrigerator (9) is placed in a UHV tube in the center of the cryostat. This tube extends from the electrical feedthroughs at the top of the cryostat to the bottom flange, where it connects to the central UHV chamber below. As visible in the magnification of the $^3$He refrigerator in Fig. 3 the tube (2) is triple-walled. This allows hot nitrogen gas with a temperature of 180 °C to be pumped through the tube walls in order to bake out the system. We reach a temperature of 115 °C at the STM and the $^3$He refrigerator. Connecting the baking/cooling tubes to the $^4$He dewar via a needle valve (17) precools the system during normal operation.

The closed single-shot $^3$He refrigerator consists of a vibrationless charcoal sorption pump (3) connected to the $^3$He pot (5) via a pumping line that passes through the 1 K pot (11). The residual heat load is shielded by a radiation shield (14) that is thermally coupled to the 1 K pot and surrounds the $^3$He pot and the STM (7). A patented design allows the whole $^3$He refrigerator to be moved from the experimental position to the exchange position over a distance of 500 mm as shown in Fig. 2.[46,47] This is realized by the vertical movement of a nut (14) on a threaded leadscrew (13) that is rotated by a motor drive outside the UHV space via a rotary feedthrough. As visible in Fig. 3 this requires two flexible capillary coils, one (15) for feeding the 1 K pot from the dewar via a needle valve (16) and one (9) for the exhaust and for pumping the 1 K pot. The same cooling line is used for cooling the sorption pump via a bypass (10).[47]

One part of the $^3$He pot pumping line is made of a flexible bellow (4), which serves as a thermal switch. When the sorption pump is heated, the increased $^3$He pressure expands this bellow by approximately 1 mm. This causes a cone (12) in the $^3$He pot to be pressed into a countercone (13) in the 1 K pot, precooling the $^3$He pot during condensation. During base temperature operation the sorption pump is cooled, the bellow contracts, and the $^3$He pot is thermally isolated. Furthermore, the bellow acts as an additional vibration-isolation element.

The STM itself (7) is mounted to the $^3$He pot via an OFHC-copper rod (6) with a length of 300 mm.[48] This rod is thermally connected to the $^3$He pot and to the STM by gold plated pressed contacts. On the STM end, the pressed contact is built as a single plug for all electrical contacts, so that the STM can be easily removed for repair, without removing the $^3$He refrigerator. All electrical connections to the STM are heat sunk at the $^4$He exhaust capillary, at the 1 K pot, at the $^3$He pot, at the copper rod, and at the STM.

For temperature measurement we use either a Cernox sensor[49,50] directly at the STM or a $RuO_2$ sensor at the $^3$He pot.[51] At base temperature, the read out of the Cernox and that of the $RuO_2$ sensor differ by only a few millikelvin, indicating excellent thermal coupling between STM and $^3$He pot. With a 3.5 $\ell$ (normal temperature and pressure) $^3$He gas charge that condenses into about 5 cc of liquid the STM can be held at a base temperature of $315\pm5$ mK for 30 h. This is achieved without pumping at the 1 K pot with the needle valve (16) left fully open. With pumping at the 1 K pot the base temperature is reduced to $262\pm5$ mK and the hold time is increased to 130 h. Since this causes additional vibrations and since a time period of 30 h is usually sufficient for high-resolution STS measurements, we achieved all of the following results in the first mode of operation. A complete tip or sample exchange typically takes less than 4 h including recondensation of $^3$He and cool-down to base temperature. During the whole exchange process the STM temperature stays below 35 K.

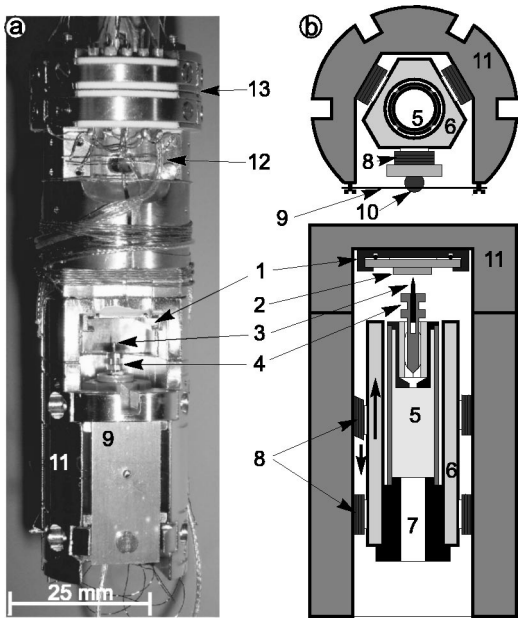


FIG. 4. (a) Photo of the STM head. (b) Horizontal (top) and vertical (bottom) cross sections. (1) Sample holder, (2) sample, (3) tip, (4) tip holder (molybdenum), (5) tube scanner, (6) sapphire prism, (7) tube scanner holder (macor), (8) shear-piezo stacks, (9) molybdenum leaf-spring, (10) titanium ball, (11) microscope body (phosphorous bronze), (12) Cernox temperature sensor, and (13) electrical connector (OFHC copper).

An additional feature of the system is the possibility to heat the $^3$He pot and the sorption pump in order to achieve higher temperatures. Below 4 K the temperature of the STM is regulated by the temperature of the sorption pump. Above 4 K, the heat load is regulated by a resistive heater on the $^3$He pot. Thereby, a wide temperature range from base temperature up to 100 K is accessible.

### C. STM head and electronics

Figure 4(a) shows a photo of the home-built STM head. It has been designed to be as small and compact as possible in order to make it less susceptible against vibrations. It measures 26 mm in diameter by 85 mm in length including the connector (13). The compactness is obtained primarily by integration of the tube scanner (5) into the coarse-approach motor as visible in Fig. 4(b). The microscope body (11) is made of phosphorous bronze, a hard, nonmagnetic, and UHV-compatible copper alloy.

The coarse approach motor is of the so-called Walker design.[52] It consists of a sapphire prism (6), which is clamped between 6 thin plates of $Al_2O_3$ glued on top of shear-piezo stacks (8).[53] The clamping is accomplished by a molybdenum leaf-spring (10) that presses the front two

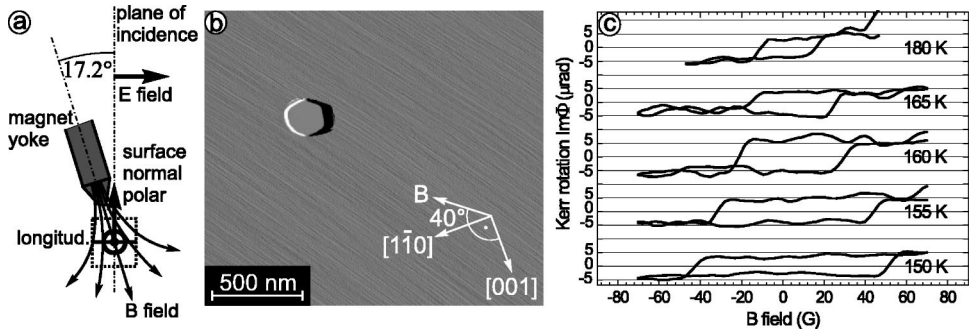


FIG. 5. (a) Geometry of the MOKE setup. The sample surface in polar geometry is represented by the black line with the surface normal pointing upwards. In longitudinal geometry the sample surface is represented by the dotted square with the surface normal perpendicular to the sheet plane. (b) Constant-current image of 1 ML Fe/W(110) annealed at 800±100 K ($I$=0.04 nA, $V$=−0.8 V). The Fe material in excess of 1 ML forms large islands on the closed Fe monolayer. (c) Hysteresis curves in longitudinal geometry of the sample in (b) measured by MOKE at temperatures close to $T_C$. The magnetic field $B$ is applied along the arrow shown in (b). The $x$ axis corresponds to the component parallel to [110].

shear-piezo stacks onto the sapphire prism. We drive the motor in stick-slip mode of operation[54] and achieve a step width of 25 nm at a voltage of 300 V at base temperature. The coarse motor is very stable and reliable at low temperature.

For scanning, a 1/4 in. piezo tube scanner[53] (5) with a length of 20 mm is mounted by use of a macor piece (7)[85] into the sapphire prism. For the five electrodes (four segments on the outer face, one on the inner) we chose copper instead of the often used nickel to avoid magnetic material. The maximum scan range with an applied voltage of ±240 V amounts to 1 $\mu$m×1 $\mu$m at base temperature and the $z$-range is calculated to be 200 nm.

As STM tips (3), we use thin wires of the desired material, which are either mechanically sharpened (Pt/Ir, Nb) or electrochemically etched (W) *ex situ*. The tip wire is then clamped into the tip holder (4), which itself is stuck into the tube scanner. By means of a transporter the tip holder can be safely transferred into the UHV system and inserted into the STM without danger of damage to the tube scanner as described elsewhere.[55] Further *in situ* tip preparation is described below.

The STM is operated by commercial control electronics and software[56] with a home-built preamplifier. Both the sample bias supply and the tunneling current measurement are done fully differentially as outlined by Züger *et al.*[57] Tip and sample are connected to the preamplifier mounted outside the UHV via shielded twisted-pair cables[58] containing both signal and reference potential line. This circuit combines a low capacitive coupling between tunneling current and bias, which is important for modulation techniques, with an effective shielding against electrical noise. To shield against high frequency noise, all in- and outputs of the preamplifier are filtered through commercial T-filters with a cutoff frequency of about 30 MHz. The preamplifier with cables has a total gain of 1 V/1 nA at a bandwidth of approximately 5 kHz, and an input current noise of 3 $pA_{rms}$.

### D. UHV system

Figure 1 shows a survey of the UHV system composed of three chambers that are separated by UHV valves. Each chamber is pumped by a 150 $\ell$/s ion getter pump including a titanium sublimation pump, connected to the chambers via a 100 mm (inner diameter) flange.[59] After baking the system including the UHV tube of the cryostat for about one week, we reach a base pressure of $p<1\times10^{-10}$ mbar in each chamber, even with the cryostat at room temperature.

In the central UHV chamber (7), STM tips and samples can be transferred into and out of the STM. From there, they are transported between the chambers by means of magnetic drives (11) and wobblesticks.[60] The second UHV chamber (8) contains several molecular beam evaporators, a room-temperature STM[61] including a resistive heater ($T_{max}$ =700 K) for easy and fast sample characterization and a combined low-energy electron diffraction (LEED)/Auger-electron spectroscopy unit.[62] The third UHV chamber (9) contains an ion source for sputtering,[63] a gas inlet for gas dosage, several metal beam evaporators, a quadrupole mass spectrometer,[64] and a home-built electron bombardment heater for tips and samples with $T_{max}>2400$ K assembled on a commercial $x,y,z$ manipulator.[60] By a load lock (12) tips and samples are easily transferred into the system without breaking UHV in the main chambers.

#### 1. Variable-temperature magneto-optical Kerr-effect-setup

The $x,y,z$ manipulator in the third UHV chamber additionally contains a stage that allows *in situ* magneto-optical Kerr-effect (MOKE) measurements at variable temperatures. The home-built MOKE setup uses a conventional laser/detector setup mounted on two viewports outside the UHV chamber. It includes a 670 nm constant-current stabilized laser diode, a polarizer, a $\lambda/4$ phase shifter, an analyzer, a color filter, and a photodiode detector. The magnetic field is generated by a single yoke electromagnet with the coil mounted outside the UHV chamber. The soft-magnetic yoke[65] is mounted inside the UHV chamber and can be moved close to the sample surface.

The geometry of the setup is shown in Fig. 5(a). The sample surface can be moved in polar as well as in longitudinal geometry in order to be sensitive to the out-of-plane and to the in-plane components of the sample magnetization, respectively. The imaginary part of the Kerr angle Im $\Phi(B)$

is measured by ramping the magnetic field and recording the output of the detector.[66,67] We achieve a maximum magnetic field of 35 mT at the sample position. Due to the restricted geometry of the UHV chamber, the axis of the yoke has an angle of 17.2° to the plane of incidence of the laser light. Consequently, the magnetic field has a small component (30%) perpendicular to the plane of incidence. Since this component is parallel to the electric field direction, the corresponding magnetization component does not enter into the measured Kerr angle.

For the purpose of variable temperatures, the sample holder includes a resistive heater and is coupled to a $^4$He continuous-flow cryostat[68] via flexible copper braids. The temperature is measured with a Si diode attached to the sample holder.[69] We achieve temperatures between 30 and 450 K.

To test the sensitivity of the MOKE setup, we prepared a 1 ML Fe film on W(110). The W(110) substrate was cleaned by repeated cycles of heating at 1500 K in an oxygen atmosphere of $5\times10^{-7}$ mbar and subsequent flashing to 2300 K.[70] The Fe film was deposited at room temperature with an e-beam evaporator at a rate of 0.5 ML/min and was subsequently thermally annealed for 10 min at $800\pm100$ K. During preparation the pressure remained below $2\times10^{-10}$ mbar. The topography of the sample is shown in Fig. 5(b). The Fe material in excess of 1 ML forms a few large islands with a height of about 35 ML which cover only 1% of the surface. On the remaining major part of the surface the substrate is covered with a closed Fe monolayer.[71]

The Kerr loops measured in longitudinal geometry with the *B*-field direction close to $[1\bar{1}0]$ are shown in Fig. 5(c). They are measured on the identical sample of (b) at different temperatures. We find squarelike hysteresis curves indicating an easy axis in the film plane. The coercivity field clearly decreases with increasing temperature. At higher temperatures, the hysteretic behavior vanishes (not shown). It is known that the Fe monolayer is ferromagnetic with a Curie temperature $T_C$ well below room temperature. It has an easy axis pointing in $[1\bar{1}0]$ direction. $T_C$ can be estimated to be 210 K given the terrace width of 10 nm.[72] On the other hand, Fe islands of the height found here are known to show a magnetic vortex structure with a $T_C$ above room temperature.[11,73] This indicates that the hysteretic signal in Fig. 5(c) originates from the Fe monolayer and not from the few islands. From the signal strength, we thus determine that the MOKE setup can easily resolve a coverage below 1 ML. Moreover, the experiment shows that the ferromagnetism of low dimensional structures, usually exhibiting a high coercivity field, can be measured with this setup by heating the sample to about $T_C$.

#### *2. Tip preparation for spin-resolved measurements*

For spin-resolved STS measurements, the tungsten STM tips are prepared *in situ* similarly to previous experiments.[11,45] We typically flash to about 2300 K, then coat with several monolayers of magnetic material and afterwards anneal for 5 min at about 500 K. A convenient sample system to test the magnetic sensitivity of our tips is the vortex domain configuration of Fe islands which are prepared as described above.[11,73] As an example, we show the domain configuration as measured with an in-plane sensitive tip obtained by coating with 5–6 ML of Fe. Figure 6(a) shows the topography of the sample and Fig. 6(b) the simultaneously recorded, spin-resolved $dI/dV$ map of the same area. These data were recorded at room temperature. We clearly observe the in-plane domains of the magnetic vortex configuration as found at 14 K,[11] proving that the tip is sensitive to the in-plane component of the magnetization.

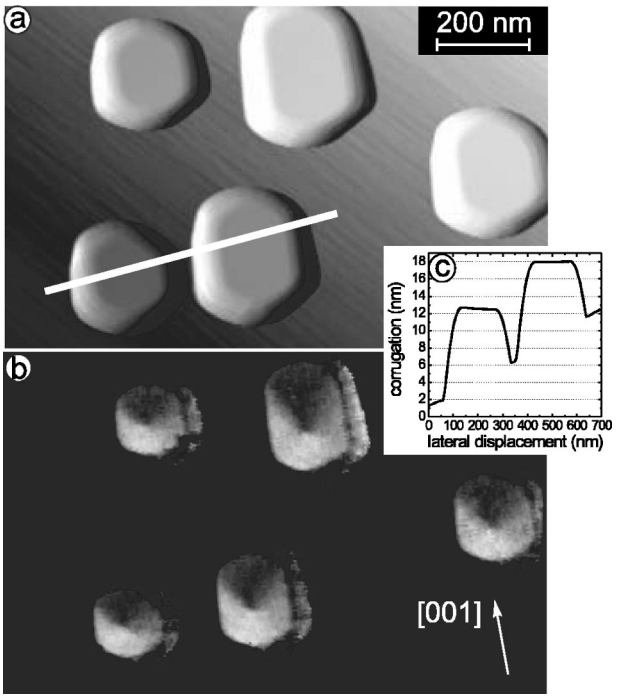


FIG. 6. (a) Constant-current image of Fe islands on W(110) measured with an Fe coated tip. (b) Simultaneously recorded, spin-resolved $dI/dV$ map showing magnetic vortex states of the Fe islands at room temperature ($I_{stab}=0.3$ nA, $V_{stab}=-0.3$ V, $V_{mod}=30$ mV$_{rms}$). (c) Line section taken along the white line in (a).

## III. EXPERIMENTAL RESULTS AT BASE TEMPERATURE

The principal tests of our facility concern the stability of the STM, the spin resolution, and the energy resolution in the STS mode at base temperature.

### A. *Z* stability

First tests of the STM were performed on *in situ* cleaved InAs single crystals. This procedure yields an atomically flat and largely defect free InAs(110) surface.[74] The *z* calibration was performed on step edges that occasionally appear on the surface.[28] The constant-current image on a small length scale is shown in Fig. 7(a). The dangling bonds of the As atoms are clearly resolved.[75] A line section taken perpendicular to the atomic rows in Fig. 7(b) reveals an atomic corrugation of about 30 pm with a *z*-noise level of 5 pm$_{pp}$. In order to demonstrate the performance in a magnetic field we imaged the same surface at 4 T as shown in Figs. 7(c) and 7(d). The *z*-noise level is still below 5 pm$_{pp}$.

Note, that these results were obtained at an early stage with a nonoptimized setup. Up to that time, there was no

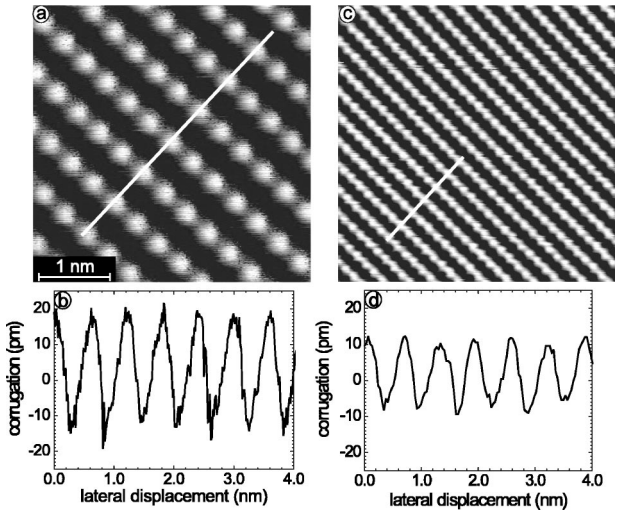


FIG. 7. (a) Constant-current image taken at 315 mK showing atomic resolution on InAs(110) (unfiltered data, $I=0.8$ nA, $V=-0.9$ V). (b) The line section along the white line in (a) shows a noise level of 5 $pm_{pp}$. (c), (d) Same as (a), (b) but in a magnetic field of 4 T (unfiltered data, $I=1.5$ nA, $V=-1$ V). Note that the atomic corrugation is reduced due to a different microtip. The noise level is still below 5 $pm_{pp}$.

sand in the aluminum barrel, no acoustic shielding and only partial electrical filtering of the STM cables. The $z$ noise could further be reduced by optimizing the setup.

### B. Spin resolution

To demonstrate our ability to perform spin-resolved measurements at 300 mK we imaged the stripe-domain structure of Fe double-layer (DL) nanowires on W(110).[45,76] The nanowires are prepared by deposition of 1.5 ML Fe at a rate of 0.5 ML/min and at a temperature of approximately 500 K. As seen in Fig. 8(a) this procedure results in a grating of alternating Fe monolayer (ML) and Fe double-layer (DL) stripes running parallel to the step edges of the W(110) substrate. In this particular measurement, we succeeded in preparing a spin-sensitive tip by gently touching the Fe surface with a tungsten tip. Figure 8(b) shows the resulting spin-resolved $dI/dV$ map recorded simultaneously with the topography in (a). A higher resolution $dI/dV$ map is shown in Fig. 8(c). We clearly observe the out-of-plane stripe domains of the Fe DL nanowires which are oriented roughly parallel to the $[1\bar{1}0]$ direction and perpendicular to the dislocation lines, as found at 14 K.[45] Obviously, our tip creates a strong out-of-plane contrast of about 30%. Fitting the domain-wall profiles as described by Kubetzka *et al.*[76] reveals a tip-magnetization angle of $10° \pm 10°$ relative to the surface normal. The fit results in a domain-wall width of $7 \pm 1$ nm which is consistent with the value found at 14 K.[76] We want to point out, that similar to voltage pulses,[77] the particular tip preparation used here is responsible for the out-of-plane sensitivity in contrast to the usual in-plane sensitivity achieved by coating with several monolayers of Fe as described in Sec. II D 2.

To our knowledge, these measurements show for the first time spin resolution in STS measurements at subkelvin temperatures. They demonstrate that the preparation of spin-sensitive tips could be quite easy at very low temperatures.

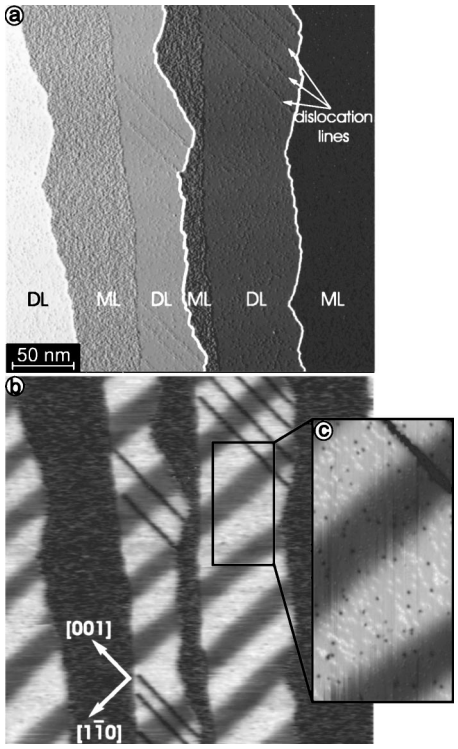


FIG. 8. Constant-current image (a) and simultaneously recorded, spin-resolved $dI/dV$ map (b) of 1.5 ML Fe/W(110) measured with an out-of-plane sensitive tip ($I_{stab}=1$ nA, $V_{stab}=0.7$ V, $V_{mod}=20$ $mV_{rms}$, $T=315$ mK). The Fe overlayer forms alternating monolayer (ML) and double-layer (DL) stripes running parallel to the step edges of the W(110) substrate. The $dI/dV$ map clearly shows the domain contrast of the DL stripes with the domain walls oriented roughly along $[1\bar{1}0]$ perpendicular to the dislocation lines marked in (a). (c) $dI/dV$ map with higher spatial resolution of the area marked in (b).

### C. Energy resolution

To demonstrate the high energy resolution of our STM we performed STS measurements on $NbSe_2$, a well-studied layered material that has a superconducting phase transition at approximately 7.2 K.[78] A $dI/dV$ map of the cleaved surface taken at a magnetic field of 0.5 T is shown in Fig. 9(a). The Abrikosov flux lattice of the type II superconductor is well resolved. Figure 9(b) shows $dI/dV$ curves measured by lock-in technique at variable temperatures in zero magnetic field. The temperature dependence of the superconducting energy gap can clearly be observed. We see a difference between the curve measured at 700 mK and the curve measured at 310 mK, i.e., an earlier onset of nonzero conductance within the gap. This indicates that our electronic tip temperature is at least below 700 mK.

Since the superconducting gap of $NbSe_2$ is anisotropic, a fit to conventional BCS theory is not possible. Therefore we also measured $dI/dV$ curves on the normal metal W(110) using a superconducting niobium tip. A similar experiment using the Au(111) surface is known to yield $dI/dV$ curves that fit well to BCS theory.[79] We used mechanically sharpened, polycrystalline Nb wires with a diameter of 0.8 mm. The W(110) surface is prepared as described in Sec. II D 1. After inserting the tip into the STM, we applied voltage pulses on the W(110) surface to remove the oxide from the tip. The $dI/dV$ curves are then measured on a clean sample

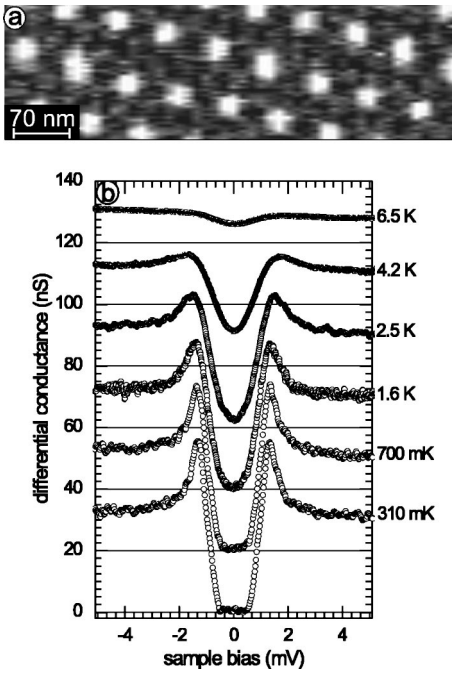


FIG. 9. (a) $dI/dV$ map of the cleaved $NbSe_2$ surface showing the Abrikosov flux lattice at a magnetic field of 0.5 T and at a sample bias of 0 mV ($I_{stab}$ =0.2 nA, $V_{stab}$=−6.8 mV, $V_{mod}$=80 $\mu V_{rms}$, $T$=310 mK). (b) $dI/dV$ curves measured by lock-in technique on $NbSe_2$ at $B$=0 T using a tungsten tip. The measurement temperature is given beside each curve. The curves are averages from several single curves taken on the same sample area; 300 mK–1.6 K: average of 2×2 curves; 2.5 K: 3×3; 4.2 K–6.5 K: 10 ×10. The curves are offset by 20 nS steps for clarity ($I_{stab}$=0.2 nA, $V_{stab}$ =6 mV, $V_{mod}$=24 $\mu V_{rms}$).

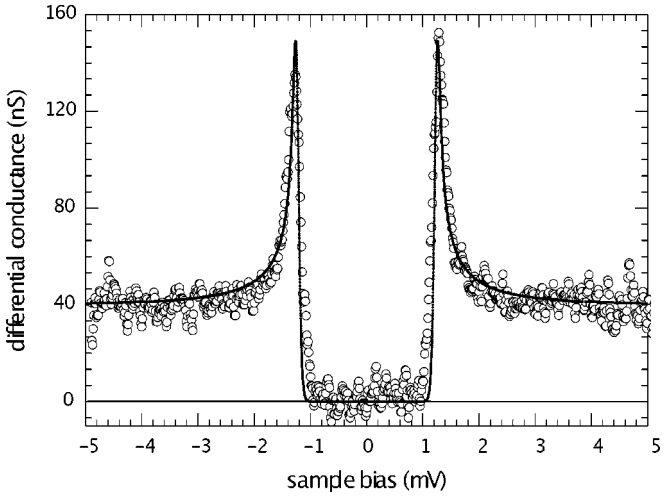


FIG. 10. Open circles: $dI/dV$ curve measured by lock-in technique with a Nb tip on a W(110) sample ($I_{stab}$=0.2 nA, $V_{stab}$=−5 mV, $V_{mod}$=20 $\mu V_{rms}$, $T$=315 mK). Solid line: fit to the experimental data revealing a superconducting energy gap of $\Delta$=1.23 meV and a fit temperature of $T_{fit}$=315 mK.

area. Figure 10 shows a $dI/dV$ curve measured at base temperature. The superconducting energy gap is clearly resolved. To determine the electronic temperature of the sample, we use the standard relation for STM $I(V)$ spectra[80–82]

$$I(V) \propto \int_{-\infty}^{\infty} \rho_s(\epsilon + eV)\rho_t(\epsilon)[f_s(\epsilon + eV) - f_t(\epsilon)]d\epsilon \qquad (1)$$

with the sample and the tip density of states $\rho_s$ and $\rho_t$ and the corresponding Fermi functions $f_s$ and $f_t$. We assume that $\rho_s$ is approximately constant in the small energy range around $E_F$[83] and use the standard BCS density of states for the tip

$$\rho_t(\epsilon) \propto \begin{cases} \dfrac{|\epsilon|}{\sqrt{\epsilon^2 - \Delta^2}} & : \ |\epsilon| > \Delta \\ 0 & : \ |\epsilon| < \Delta \end{cases} \qquad (2)$$

with the superconducting energy gap $\Delta$.[84] The detection of the differential conductivity via lock-in amplifier with a modulation voltage of $V_{mod}$=20 $\mu V_{rms}$ is then taken into acount by numerically integrating

$$\frac{dI}{dV}(V) \propto \int_{-\pi/2}^{\pi/2} \sin\alpha \times I(V + \sqrt{2}\, V_{mod} \times \sin\alpha)d\alpha. \qquad (3)$$

The resulting curve is fitted to our data by adjusting the energy gap $\Delta$ and the temperature $T_{fit}$ of the Fermi function. The measured energy gap $\Delta$ depends on the microtip, i.e., it can change after field emission, as already described by Pan *et al.*[79] We find that this effect results in a variation of the gap by approximately ±10%. The fit result is shown in Fig. 10 as a solid line revealing a fit temperature of $T_{fit}$=315 mK and an energy gap of $\Delta$=1.23 meV. The same procedure was carried out for several different measurements using different microtips and different stabilization currents resulting in an average sample temperature of $T_{fit}$=350±35 mK. This is only slightly higher than the sample temperature read from the Cernox sensor on the STM head indicating that our energy resolution is close to the thermal limit of $3.3kT$=85 $\mu$eV.

## ACKNOWLEDGMENTS

The authors thank the mechanical workshop of the Institute of Applied Physics for helpful technical discussions and for machining the STM, most parts of the UHV system, and parts of the frame. The authors also thank E. Groß from the TU Hamburg-Harburg for cooperation during the design of the frame. The authors acknowledge financial support from SFB 508-B4, Wi 1277/15, and Graduiertenkolleg "Physik nanostrukturierter Festkörper" of the "Deutsche Forschungsgemeinschaft."

[1] R. Wiesendanger, *Scanning Probe Microscopy and Spectroscopy* (Cambridge University Press, Cambridge, 1994).
[2] C. J. Chen, *Introduction to Scanning Tunneling Microscopy* (Oxford University Press, New York, 1993).
[3] *Scanning Tunneling Microscopy and Spectroscopy Theory, Techniques, and Applications*, edited by D. A. Bonnell (VCH Publishers, New York, 1993).
[4] X. L. Wu and C. M. Lieber, Science **243**, 1703 (1989).
[5] J. M. Carpinelli, H. H. Weitering, E. W. Plummer, and R. Stumpf, Nature (London) **381**, 398 (1996).
[6] J. Li, W.-D. Schneider, R. Berndt, and B. Delley, Phys. Rev. Lett. **80**, 2893 (1998).
[7] H. C. Manoharan, C. P. Lutz, and D. M. Eigler, Nature (London) **403**, 512 (2000).
[8] V. Madhavan, W. Chen, T. Jamneala, M. F. Crommie, and N. S. Wingreen, Science **280**, 567 (1998).
[9] S. H. Pan *et al.*, Nature (London) **413**, 282 (2001).
[10] B. W. Hoogenboom, K. Kadowaki, B. Revaz, M. Li, Ch. Renner, and Ø. Fischer, Phys. Rev. Lett. **87**, 267001 (2001).
[11] A. Wachowiak, J. Wiebe, M. Bode, O. Pietzsch, M. Morgenstern, and R. Wiesendanger, Science **298**, 577 (2002).

[12] H. Yang, A. R. Smith, M. Prikhodko, and W. R. L. Lambrecht, Phys. Rev. Lett. **89**, 226101 (2002).
[13] T. K. Yamada, M. M. J. Bischoff, M. M. Heijnen, T. Mizoguchi, and H. van Kempen, Phys. Rev. Lett. **90**, 056803 (2003).
[14] U. Schlickum, N. Janke-Gilman, W. Wulfhekel, and J. Kirschner, Phys. Rev. Lett. **92**, 107203 (2004).
[15] D. C. Tsui, H. L. Stormer, and A. C. Gossard, Phys. Rev. Lett. **48**, 1559 (1982).
[16] E. Abrahams, S. V. Kravchenko, and M. Sarachik, Rev. Mod. Phys. **73**, 251 (2001).
[17] Z. Fisk, D. W. Hess, C. J. Pethick, D. Pines, J. L. Smith, J. D. Thompson, and J. O. Willis, Science **239**, 33 (1988).
[18] M. Jourdan, M. Huth, and H. Adrian, Nature (London) **398**, 47 (1999).
[19] T. M. Risemann *et al.*, Nature (London) **396**, 242 (1998).
[20] K. Ishida, H. Mukuda, Y. Kitaoka, K. Asayama, Z. Q. Mao, Y. Mori, and Y. Maeno, Nature (London) **396**, 658 (1998).
[21] B. I. Barker, S. K. Dutta, C. Lupien, P. L. McEuen, N. Kikuagawa, Y. Maeno, and J. C. Davis, Physica B **329**, 1334 (2003).
[22] D. Grundler, Phys. Rev. Lett. **84**, 6074 (2000).
[23] T. Matsuyama, R. Kürsten, C. Meißner, and U. Merkt, Phys. Rev. B **61**, 15588 (2000).
[24] J. Nitta, T. Akazaki, H. Takayanagi, and T. Enoki, Phys. Rev. Lett. **78**, 1335 (1997).
[25] M. Morgenstern, J. Klijn, Chr. Meyer, M. Getzlaff, R. A. Adelung, R. Römer, K. Rossnagel, L. Kipp, M. Skibowski, and R. Wiesendanger, Phys. Rev. Lett. **89**, 136806 (2002).
[26] M. Morgenstern, J. Klijn, Chr. Meyer, and R. Wiesendanger, Phys. Rev. Lett. **90**, 056804 (2003).
[27] J. Wiebe, Chr. Meyer, J. Klijn, M. Morgenstern, and R. Wiesendanger, Phys. Rev. B **68**, 041402 (2003).
[28] Chr. Meyer, J. Klijn, M. Morgenstern, and R. Wiesendanger, Phys. Rev. Lett. **91**, 076803 (2003).
[29] K. Kanisawa, M. J. Butcher, Y. Tokura, H. Yamaguchi, and Y. Hirayama, Phys. Rev. Lett. **87**, 196804 (2001).
[30] B. Huckestein, B. Kramer, and L. Schweitzer, Surf. Sci. **263**, 125 (1992).
[31] A. P. Fein, J. R. Kirtley, and R. M. Feenstra, Rev. Sci. Instrum. **58**, 1806 (1987).
[32] J. W. G. Wildöer, A. van Oudenaarden, C. J. P. M. Harmans, and H. van Kempen, J. Vac. Sci. Technol. B **16**, 2837 (1998).
[33] S. H. Pan, E. W. Hudson, and J. C. Davis, Rev. Sci. Instrum. **70**, 1459 (1999).
[34] M. Kugler, Ch. Renner, Ø. Fischer, V. Mikheev, and G. Batey, Rev. Sci. Instrum. **71**, 1475 (2000).
[35] A. J. Heinrich, C. P. Lutz, J. A. Gupta, and D. M. Eigler, AIP Conf. Proc. **696**, 100 (2003).
[36] H. F. Hess, R. B. Robinson, and J. V. Waszczak, Physica B **169**, 422 (1991).
[37] P. Davidsson, H. Olin, M. Persson, and S. Pehrson, Ultramicroscopy **42–44**, 1470 (1992).
[38] H. Fukuyama, H. Tan, T. Handa, T. Kumakura, and M. Morishita, Czech. J. Phys. **46**, 2847 (1996).
[39] T. Matsui, H. Kambara, and H. Fukuyama, J. Low Temp. Phys. **121**, 803 (2000).
[40] T. Matsui, H. Kambara, I. Ueda, T. Shishido, Y. Miyatake, and H. Fukuyama, Physica B **329**, 1653 (2003).
[41] S. H. Pan, E. W. Hudson, K. M. Lang, H. Eisaki, S. Uchida, and J. C. Davis, Science **285**, 88 (1999).
[42] E. W. Hudson, K. M. Lang, V. Madhavan, S. H. Pan, H. Eisaki, S. Uchida, and J. C. Davis, Nature (London) **411**, 920 (2001).
[43] M. Kugler, Ch. Renner, V. Mikheev, G. Batey, and Ø. Fischer, Physica B **280**, 551 (2000).
[44] S. Heinze, M. Bode, A. Kubetzka, O. Pietzsch, X. Nie, S. Blügel, and R. Wiesendanger, Science **288**, 1805 (2000).
[45] A. Kubetzka, M. Bode, O. Pietzsch, and R. Wiesendanger, Phys. Rev. Lett. **88**, 057201 (2002).
[46] V. Mikheev, United States Patent No. 5829270 (Nov 3, 1998).
[47] G. Batey and V. Mikheev, J. Low Temp. Phys. **113**, 933 (1998).
[48] OFHC copper (oxygen free high conductivity).
[49] Cernox-1030-SD-HT. Lake Shore Cryotronics, Westerville, Ohio.
[50] Cryophysics GmbH. D-64293 Darmstadt, Germany.
[51] Oxford Instruments Superconductivity, Research Instruments, Tubney Woods, Oxon OX13 5QX, United Kingdom.
[52] S. H. Pan, International Patent Publication No. WO 93/19494 (International Bureau, World Intellectual Property Organization), September 30, 1993.
[53] EBL#4. Stavely Sensors Inc., East Hartford, CT 06108.
[54] G. Mariotto, M. D. Angelo, and I. V. Shvets, Rev. Sci. Instrum. **70**, 3651 (1999).
[55] O. Pietzsch, A. Kubetzka, D. Haude, M. Bode, and R. Wiesendanger, Rev. Sci. Instrum. **71**, 424 (2000).
[56] Scala SPM control unit. Omicron NanoTechnology GmbH, D-65232 Taunusstein, Germany.
[57] O. Züger, H. P. Ott, and U. Dürig, Rev. Sci. Instrum. **63**, 5634 (1992).
[58] Capton-isolated stainless-steel cables. ISOTEC Kabel GmbH, D-22844 Norderstedt, Germany.
[59] Noble Diode. Varian GmbH, 64289 Darmstadt, Germany.
[60] Thermo Vacuum Generators, Hastings TN38 9NN, United Kingdom.
[61] Ch. Witt, U. Mick, M. Bode, and R. Wiesendanger, Rev. Sci. Instrum. **68**, 1455 (1997).
[62] Spectaleed optic. Omicron NanoTechnology GmbH, D-65232 Taunusstein, Germany.
[63] IQE11/35. SPECS GmbH, D-13355 Berlin, Germany.
[64] Transpector C100M. Inficon, East Syracuse, New York 13057-9714.
[65] Vacofer S1. Registered trade mark of the company Vacuum Schmelze, D-63450 Hanau, Germany.
[66] F. Meier, Diploma thesis, Institut of Applied Physics, University of Hamburg, Germany (2002).
[67] J. Wiebe, Ph.D. thesis, Institute of Applied Physics, University of Hamburg, Germany (2003).
[68] Konti cryostat. CryoVac GmbH & Co. KG, D-53842 Troisdorf, Germany.
[69] DT 670C-SD. Lake Shore Cryotronics, Westerville, Ohio.
[70] M. Bode, R. Pascal, and R. Wiesendanger, Surf. Sci. **344**, 185 (1995).
[71] U. Gradmann, G. Liu, H. J. Elmers, and M. Przybylski, Hyperfine Interact. **57**, 1845 (1990).
[72] H.-J. Elmers, in *Magnetische Schichtsysteme* (Kapitel B1. Ferienkurse Forschungszentrum Jülich, 1999).
[73] M. Bode, A. Wachowiak, J. Wiebe, A. Kubetzka, M. Morgenstern, and R. Wiesendanger, Appl. Phys. Lett. **84**, 948 (2004).
[74] M. Morgenstern, D. Haude, V. Gudmundsson, Chr. Wittneven, R. Dombrowski, Chr. Steinebach, and R. Wiesendanger, J. Electron Spectrosc. Relat. Phenom. **109**, 127 (2000).
[75] J. Klijn, L. Sacharow, Chr. Meyer, S. Blügel, M. Morgenstern, and R. Wiesendanger, Phys. Rev. B **68**, 205327 (2003).
[76] A. Kubetzka, O. Pietzsch, M. Bode, and R. Wiesendanger, Phys. Rev. B **67**, 020401 (2003).
[77] T. K. Yamada, M. M. J. Bischoff, T. Mizoguchi, and H. van Kempen, Appl. Phys. Lett. **82**, 1437 (2003).
[78] H. F. Hess, R. B. Robinson, R. C. Dynes, J. J. M. Valles, and J. V. Waszczak, Phys. Rev. Lett. **62**, 214 (1989).
[79] S. H. Pan, E. W. Hudson, and J. C. Davis, Appl. Phys. Lett. **73**, 2992 (1998).
[80] J. Bardeen, Phys. Rev. Lett. **6**, 57 (1961).
[81] J. Tersoff and D. R. Hamann, Phys. Rev. Lett. **50**, 1998 (1983).
[82] J. Tersoff and D. R. Hamann, Phys. Rev. B **31**, 805 (1985).
[83] M. Bode, R. Pascal, and R. Wiesendanger, J. Vac. Sci. Technol. A **15**, 1285 (1997).
[84] D. R. Tilley and J. Tilley, *Superfluidity and Superconductivity* (Institute of Physics, London, 1990).
[85] Macor. Registered trade mark of the company Corning Glass Works, New York.